Polymer Testing 104 (2021) 107383

Contents lists available at ScienceDirect

Polymer Testing

journal homepage: www.elsevier.com/locate/polytest

Reprocessable and healable ethylene copolymer/f-rGO nanocomposites crosslinked by Diels-Alder adducts with infrared- and thermo-responsive behavior

Kyung Hee Kang [a], Young-Wook Chang [a,b,*], Mohammad Sabzi [a,c]

[a] Polymer Nano Materials Laboratory, Department of Materials and Chemical Engineering, Hanyang University, Ansan, 15588, Republic of Korea
[b] BK21 FOUR ERICA-ACE Center, Hanyang University, Ansan, 15588, Republic of Korea
[c] Department of Chemical Engineering, Faculty of Engineering, University of Maragheh, Maragheh, 55181-83111, Iran

ARTICLE INFO

Keywords:
Shape memory polymer
Thermo-healing polymer
Recyclable polymer
Near infrared light induced SM polymer
Diels-alder reaction
Thermo-reversible

ABSTRACT

In this work, multi-stimuli responsive nanocomposites with recyclability and rapid healability features were developed by simultaneous incorporation of thermo-reversible DA bonds and functionalized reduced graphene oxide (f-rGO) into ethylene copolymer (G-PE). Reversible formation-dissociation of DA crosslinks was investigated by FTIR, ^{1}H NMR, DSC, and solubility test. It was observed that mechanical properties of the matrix were noticeably improved (modulus ca. 220%, tensile strength ca. 308%, and elongation at break ca. 125%) with loading a quite low amount of f-rGO (0.05 wt%). Interestingly, the results revealed the re-workability of the developed materials with no significant differences in their mechanical properties as well as shape memory (SM) effect after two cycle of melt-reprocessing. Besides, nanocomposites showed scratch-healing and excellent shape recovery under direct heating as well as near infrared light (NIR).

1. Introduction

Shape memory polymers (SMPs) are an important category of smart materials that can recover their original shape from deformed shape(s) upon exposure to an external stimulus, such as heat [1–9], infrared light [10,11], electricity [9,12–15], alternating magnetic field [16], radio frequency [17], and water [18,19].

Chemically crosslinked SMPs often exhibit superior properties, such as higher modulus and strength, better dimensional and thermal stability, and more solvent resistance as compared with non-crosslinked thermoplastic SMPs. For example, a series of thermoset SMPs based on natural rubber [20,21] and polyolefin [22] with excellent properties have been introduced. However, once the chemical networks of thermoset SMPs are formed, they cannot be generally reprocessed and recycled, and thus their permanent shape is not changeable, which can limit the use of thermoset SMPs in various applications and result in environmental issues due to their non-recyclability.

Recently, incorporation of reversible covalent bonds into thermoset SMPs is a straightforward strategy to overcome these drawbacks [23–25]. Besides that, the dissociation and reformation of dynamic crosslink bonds can endow thermo-healing feature to this kind of SMPs [10,26,27]. Among them, the chemically crosslinked SMPs based on dynamic Diels-Alder (DA) chemistry between maleimide and furfuryl groups have drawn much attention of the current researches [23,28]. However, most of the developed DA crosslinked thermo-reversible materials are based on biodegradable polymers, such pol as poly(lactic acid) (PLA) [25], polycaprolactone (PCL) [27], and polyurethane (PU) [11,26]. Interestingly, crosslinking of the conventional polymers such as polyolefins and polyacrylates with DA adducts is quite rare in literature [29], while, they are widely used in various industries. Therefore, it is necessary to develop novel reprocessable and recyclable SMPs based on conventional polymers. For instance, reprocessable and healable triple-SMPs based on ionically cross-linked syndiotactic polypropylene (PP) [30] have been successfully developed by Raidt and coworkers.

Hence, the main goal of our present work is chemical crosslinking of glycidyl containing ethylene copolymer (G-PE) with end-carboxylated DA adduct. DA adduct can form dynamic covalent crosslink points, and endow shape memory and healability features along with recyclability to the G-PE matrix. Furthermore, a series of nanocomposites containing various contents of octadecylamine functionalized reduced

* Corresponding author. Polymer Nano Materials Laboratory, Department of Materials and Chemical Engineering, Hanyang University, Ansan, 15588, Republic of Korea.
E-mail address: ywchang@hanyang.ac.kr (Y.-W. Chang).

https://doi.org/10.1016/j.polymertesting.2021.107383
Received 23 December 2020; Received in revised form 12 July 2021; Accepted 12 October 2021
Available online 13 October 2021

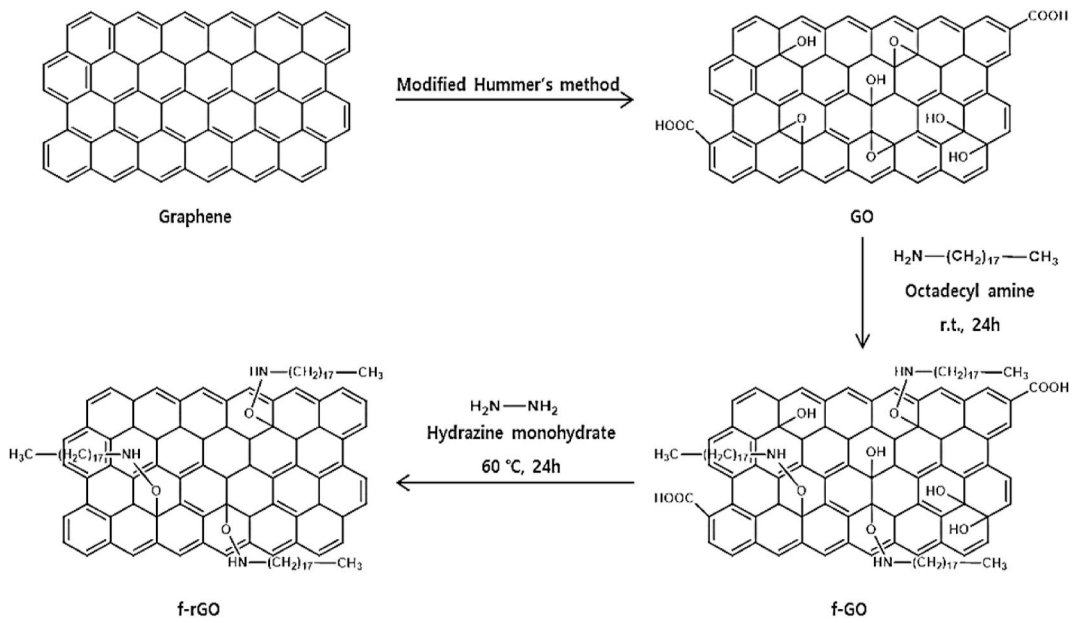

Fig. 1. Schematic representation of synthesis of f-rGO nanoplatelets.

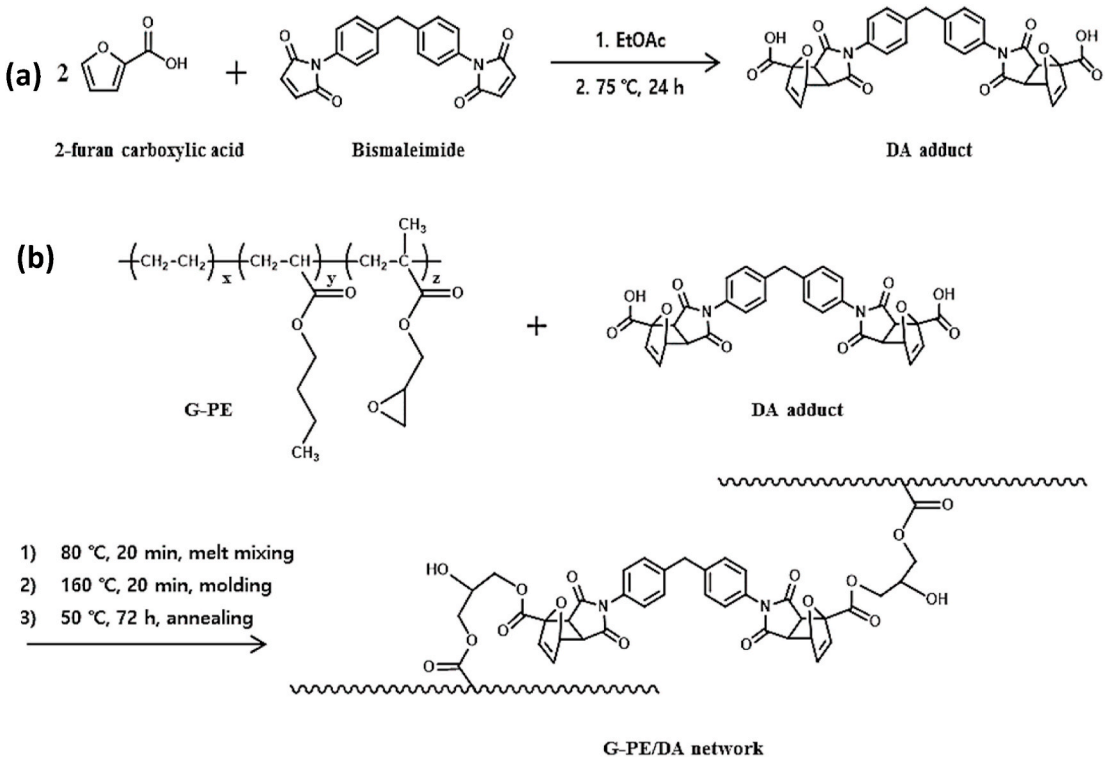

Fig. 2. Schematic demonstration of (a) the synthesis of end-carboxylated DA adduct and (b) the preparation process of G-PE/DA network.

graphene oxide (f-rGO) were prepared by melt blending method. We expect that the incorporation of robust and elastic f-rGO nanoplatelets not only will improve the thermally triggered SM and healing properties of the matrix, but also they can act as nanoheaters and provide near infrared (NIR) light responsiveness to the nanocomposites [10,31].

2. Experimental

2.1. Materials

2-Furan carboxylic acid (>98%), 4, 4′-bismaleimido-diphenylmethane (bismaleimide, ≥98.5%), and hydrazine monohydrate (>98%) were obtained from Tokyo Chemical Industry Co., Ltd. Ethyl acetate (EtOAc, ≥96.0%) was purchased from Samchun Pure Chemical Co., LTd. Ethylene-butyl acrylate-glycidyl methacrylate terpolymer (G-PE, 28% acrylate) with a melt flow index of 12 g/10 min (190 °C, 2.16 kg) was

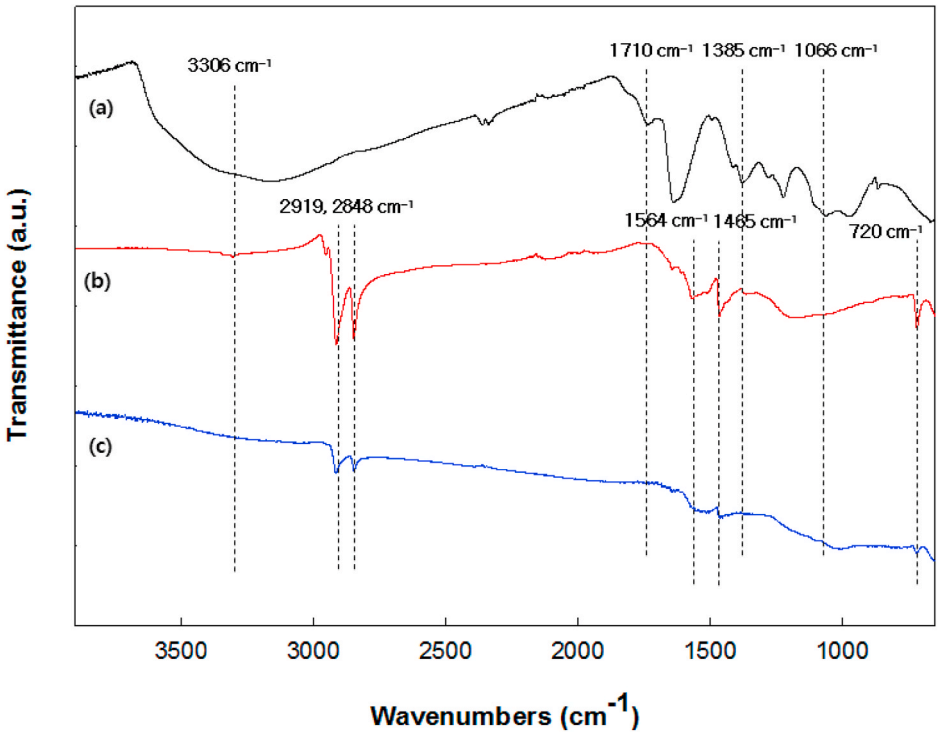

Fig. 3. FT-IR spectra of (a) GO, (b) f-GO, and (c) f-rGO.

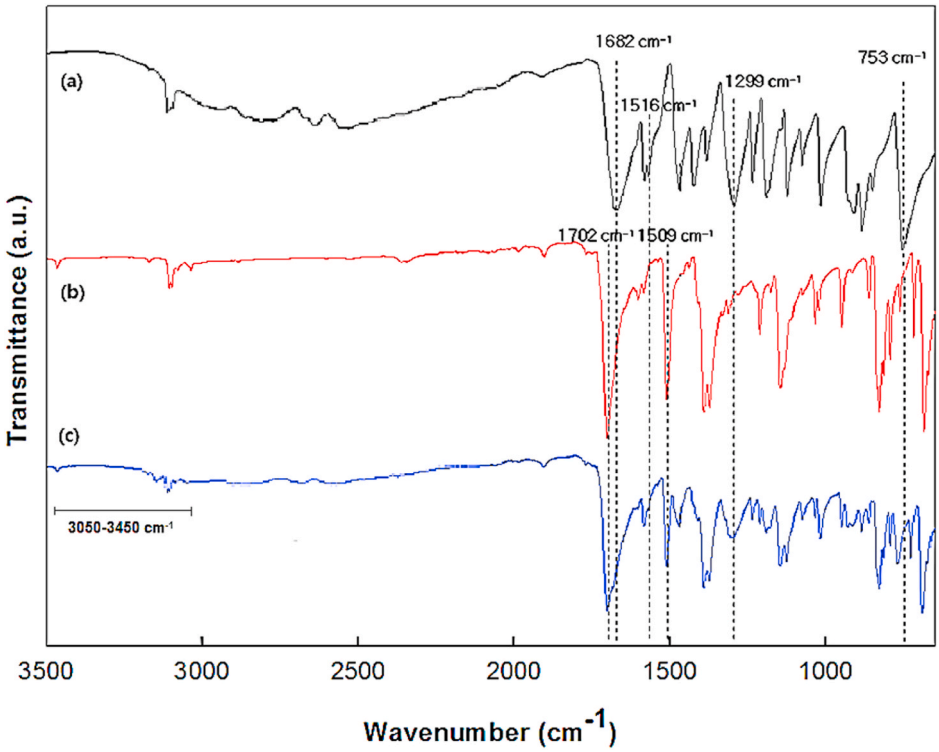

Fig. 4. FT-IR spectra of (a) 2-furan carboxylic acid, (b) bismaleimide, and (c) DA adduct.

purchased from Dupont Co. (USA) under a trade name of Elvaloy PTW. Dicumyl peroxide DCP (98%) was obtained from Aldrich. Graphite (grade 282863 with a dimension of 20 μm) and octadecylamine (99%) were obtained from Aldrich. A concentrated hydrochloric acid aqueous solution (HCl, 36.5%), a concentrated sulfuric acid aqueous solution (H_2SO_4, 95–98%), and potassium permanganate ($KMnO_4$) were purchased from Daejung Chemicals and Metals Co., Ltd. Ethanol (99.7%) and acetonitrile were supplied from Samchun Pure Chemical Co., Ltd.

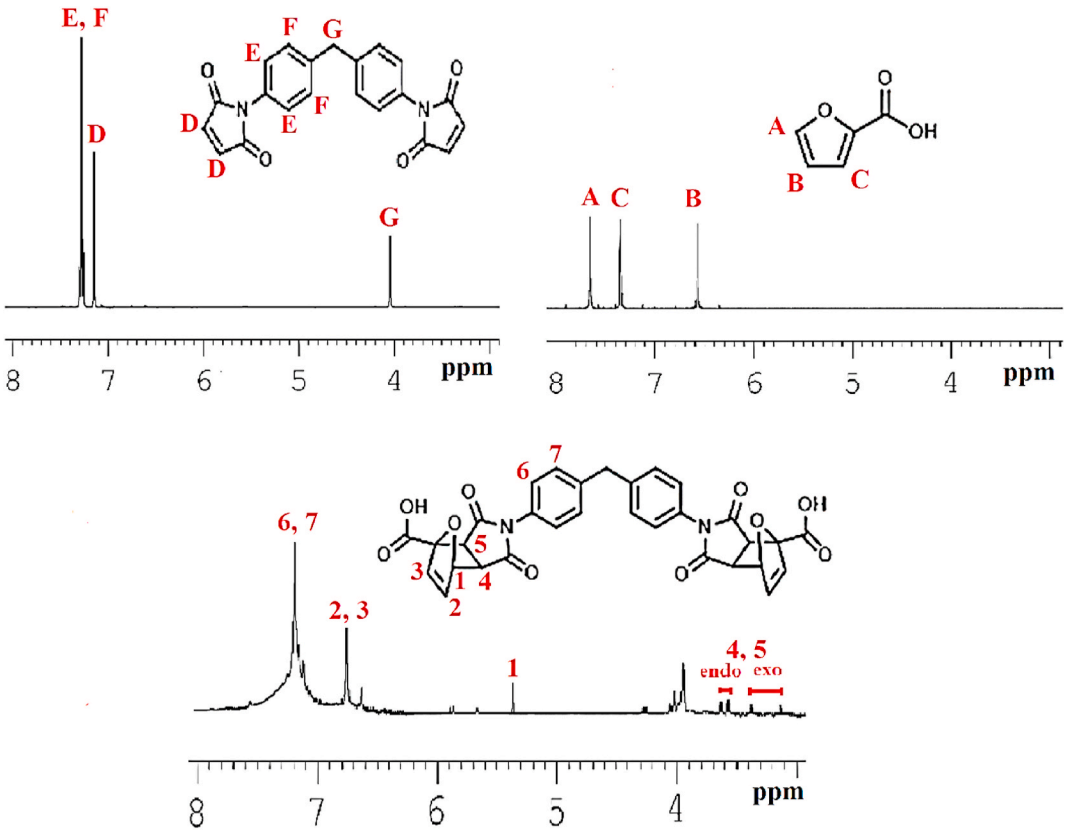

Fig. 5. ^{1}H NMR spectra of 2-furan carboxylic acid, bismaleimide, and DA adduct.

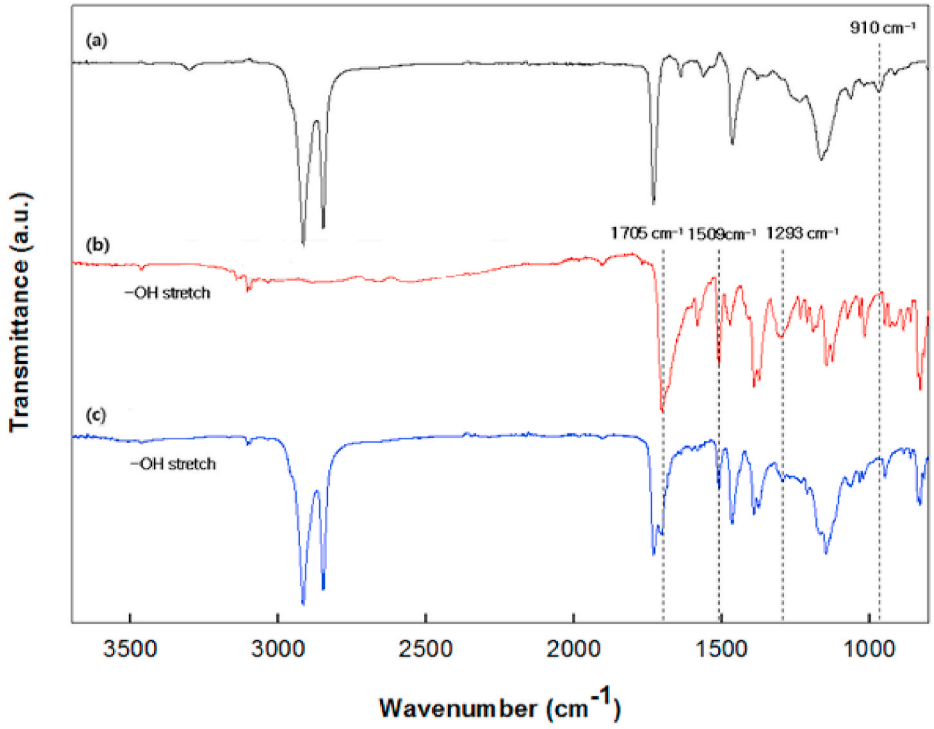

Fig. 6. FT-IR spectra of (a) neat G-PE, (b) DA adduct, and (c) G-PE/DA20.

2.2. Synthesis of f-rGO

Graphene oxide (GO) was synthesized through the modified Hummer's method [32]. Then, the surface of GO was modified by octadecylamine (ODA) [32]. Briefly, GO (2.00 g) was first dispersed in 200 ml deionized water with the aid of sonication. Meanwhile, ODA

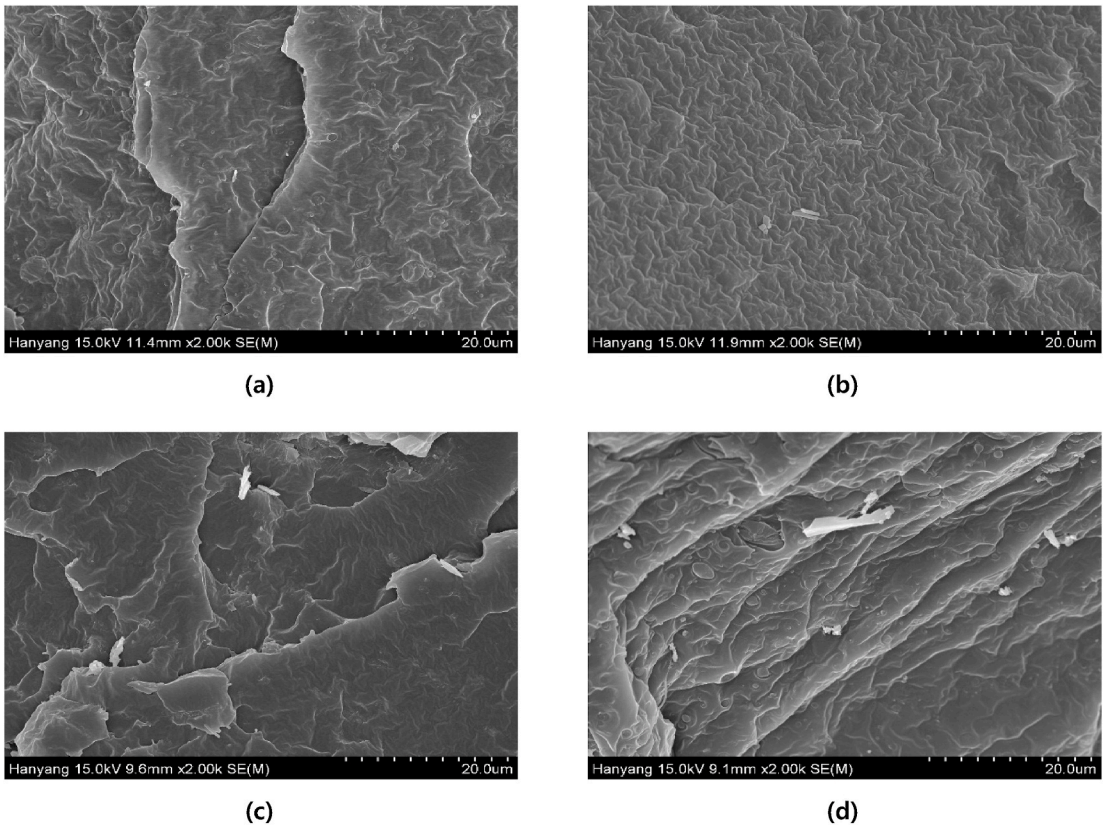

Fig. 7. FE-SEM images of G-PE/DA/f-rGO nanocomposites with (a) 0.05, (b) 0.1, (c) 0.3, and (d) 0.5 wt% of f-rGO contents.

(3.00 g) was dissolved in 100 ml ethanol and dropwise added into the GO suspension. The resultant solution was stirred at ambient temperature for 24 h. Hydrazine monohydrate (20 ml), as a reducing agent, was added and refluxed at 60 °C for 24 h. The obtained suspension was filtered and rinsed with deionized water and ethanol for at least 5 times to eliminate residual ODA and hydrazine monohydrate. Finally, the products were dried at 80 °C for 24 h to obtain octadecylamine functionalized reduced graphene oxide (f-rGO) powder, as schematically shown in Fig. 1.

2.3. Synthesis of carboxylated DA adduct

The carboxylated DA adduct was prepared using a similar method reported in the literature [33]. 2-Furan carboxylic acid (10.00 g, 89.21 mmol) and bismaleimide (16.32 g, 45.54 mmol) were dissolved in EtOAc (200 ml). The reaction was proceeded at 75 °C for 24 h in a reflux condenser to form DA bonds (Fig. 2 (a)). After cooling the resultant solution to room temperature, it was concentrated with a rotary evaporator and purified by flash chromatography using acetonitrile/EtOAc = 2:1. A white powder of carboxylated DA adduct (8.83 g, 34.10%) was obtained after drying in a vacuum oven for over 72 h at 30 °C.

2.4. Crosslinking of G-PE using carboxylated DA adduct

Before use, G-PE was first put in a vacuum oven for overnight to completely dry. A series of G-PE/DA formulations with DA adduct contents of 10, 15, and 20 phr were prepared by melt blending (Table S1). After melting of G-PE for 5 min, DA adduct was added and melt blended at 80 °C for 20 min through a Haake internal mixer (60 rpm). The resultant samples were then molded as sheets at 160 °C for 20 min to accomplish the reaction between the glycidyl groups of G-PE and the carboxylic acid groups of DA adduct [34], as schematically shown in Fig. 2 (b). After that, the sheets were thermally annealed at 50 °C for 3 days, during which the broken DA bonds within the processing at high temperature can be re-associated.

For comparison, G-PE crosslinked with DCP was also prepared with the similar method used for G-PE/DA formulations. Moreover, a series of G-PE/DA/f-rGO nanocomposites containing 0.05, 0.1, 0.3, and 0.5 wt% of f-rGO were prepared with the same protocol, except that f-rGO was loaded during mixing in the internal mixer to obtain G-PE/DA/f-rGO nanocomposites (Table S1). Reprocessed samples were prepared by cutting the sheets into small pieces and compression molding with the same condition and annealing at 50 °C for 3 days.

2.5. Characterization and measurements

2.5.1. Fourier-transform infrared spectrometer (FT-IR)

A Bucker ALPHA FT-IR spectrometer (Nicolet iS10, Thermo Scientific) was utilized to investigate the structure of synthesized materials in a range of 600–4000 cm^{-1}.

2.5.2. ^1H Nuclear magnetic resonance (NMR)

The chemical structure of DA adduct was investigated by ^1H NMR (Bruker model digital AVANCE III 400, Bruker BioSpin AG, USA) at room temperature in $CDCl_3$ as a solvent.

2.5.3. Differential scanning calorimetry (DSC)

A TA Instruments DSC Q20 was utilized to measure potential thermal transitions of G-PE/DA network and its nanocomposites. The samples were first heated from 0 to 90 °C with a scanning rate of 10 °C/min under N_2 atmosphere, then kept isothermal for 5 min, followed by cooling down to 0 °C at a scanning rate of 10 °C/min, and then heated again to 180 °C with the same scanning rate.

2.5.4. Tensile test

Tensile properties of G-PE/DA samples were measured by using a

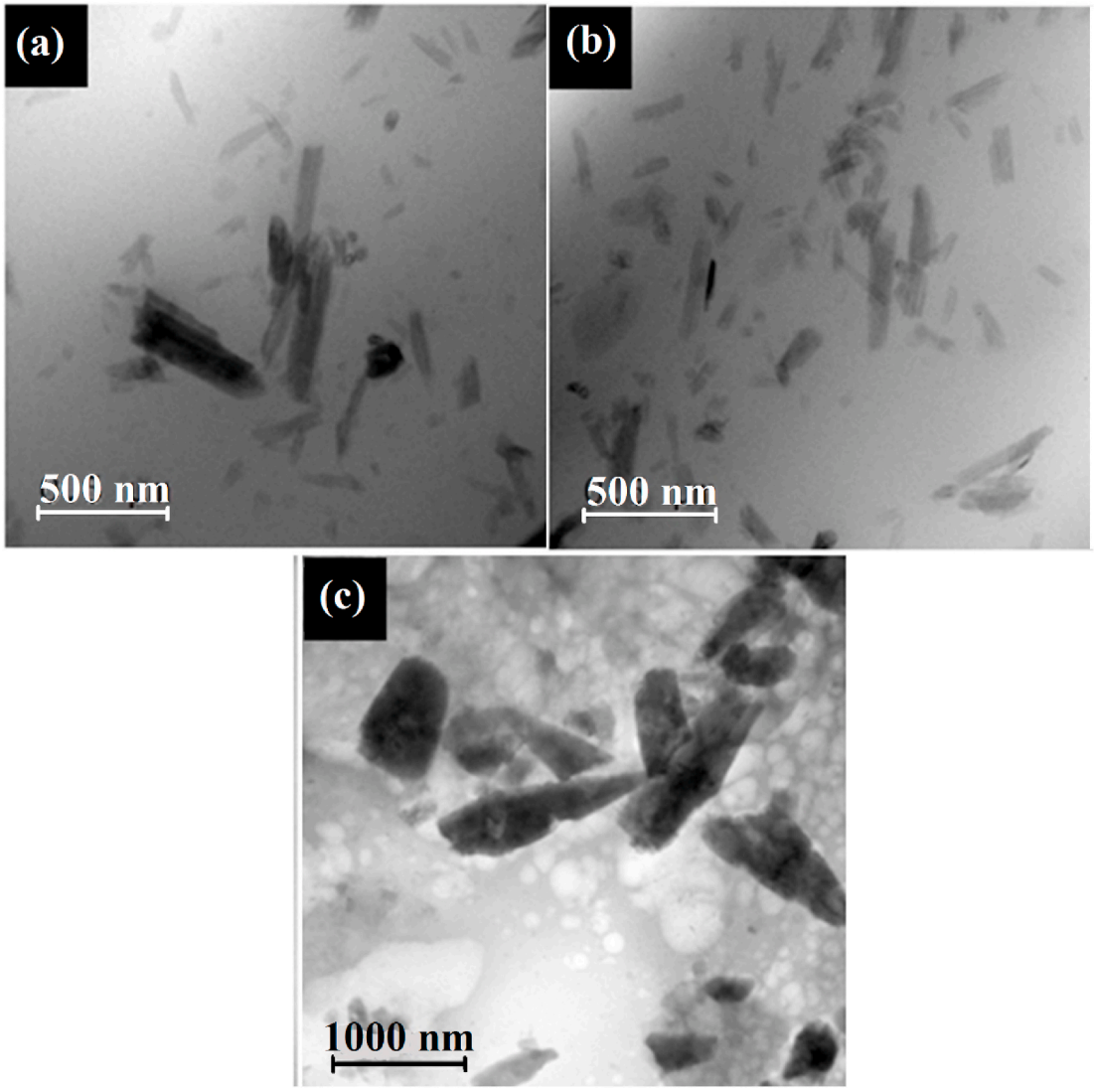

Fig. 8. FE-TEM images of G-PE/DA/f-rGO nanocomposites with (a) 0.1, (b) 0.3, and (c) 0.5 wt% of f-rGO contents.

universal testing machine (UTM, AGS-500NX, Shimadzu). The specimens were stretched until break at a speed of 50 mm/min. For each sample, the test was repeated at least five times.

2.5.5. Dynamic mechanical analysis (DMA)

The dynamic mechanical properties of the ternary blends were investigated using a dynamic mechanical analyzer apparatus (DMA-Q800, TA Instruments) with a dynamic strain of 0.2% and preloading force of 0.01 N in tensile mode at an operating frequency of 1 Hz. Rectangular specimens ($30.0 \times 6.5 \times 1.0\ mm^3$) were heated from −20 to 200 °C with a rate of 2 °C/min in N_2 atmosphere.

The crosslinking density of samples (υ_d) can be assessed from the value of storage modulus at the rubbery plateau based on equation (1) [35].

$$\upsilon_d = \frac{E'}{3RT} \tag{1}$$

where υ_d is crosslink density indicating moles of elastically effective network chains per cm^3 of sample. R and T denote the ideal gas constant and the absolute temperature that E′ was chosen.

2.5.6. Scanning electron microscopy (SEM)

Scanning electron microscopy (SEM, VEGA II, TESCAN, Czech) at an accelerating voltage of 20 kV was used to investigate the healing behavior of samples. The samples were investigated after sputter coating with a thin platinum layer.

2.5.7. Field emission-scanning electron microscopy (FE-SEM)

The cross-sectional morphology of samples was investigated by using a field-emission SEM (FE-SEM, Hitachi Co, S-900) at an accelerating voltage of 15 kV. Samples were quenched and fractured in liquid nitrogen, followed by sputter coating of the fractured surfaces a thin layer of platinum before FE-SEM observations.

2.5.8. Transmission electron microscopy (FE-TEM)

The dispersion state of the prepared ODA-GO nanoparticles within the polymer matrix was examined by FE-TEM (JEOL JEM-2100F, Japan) operating at a voltage of 200 kV. An ultra-thin slice (100 nm) of samples was cut using a cryo-microtome (Reichert Ultracut, Leica Microsystem GmbH, Nussloch, Germany) and put on copper grids coated with carbon–formvar.

2.5.9. Thermally triggered shape memory effect

For visual shape memory experiment in bending mode, a rectangular shape of samples was cut ($50 \times 10 \times 1\ mm^3$). Firstly, the samples were kept at 80 °C (which is well above the T_m of all samples) for 5 min,

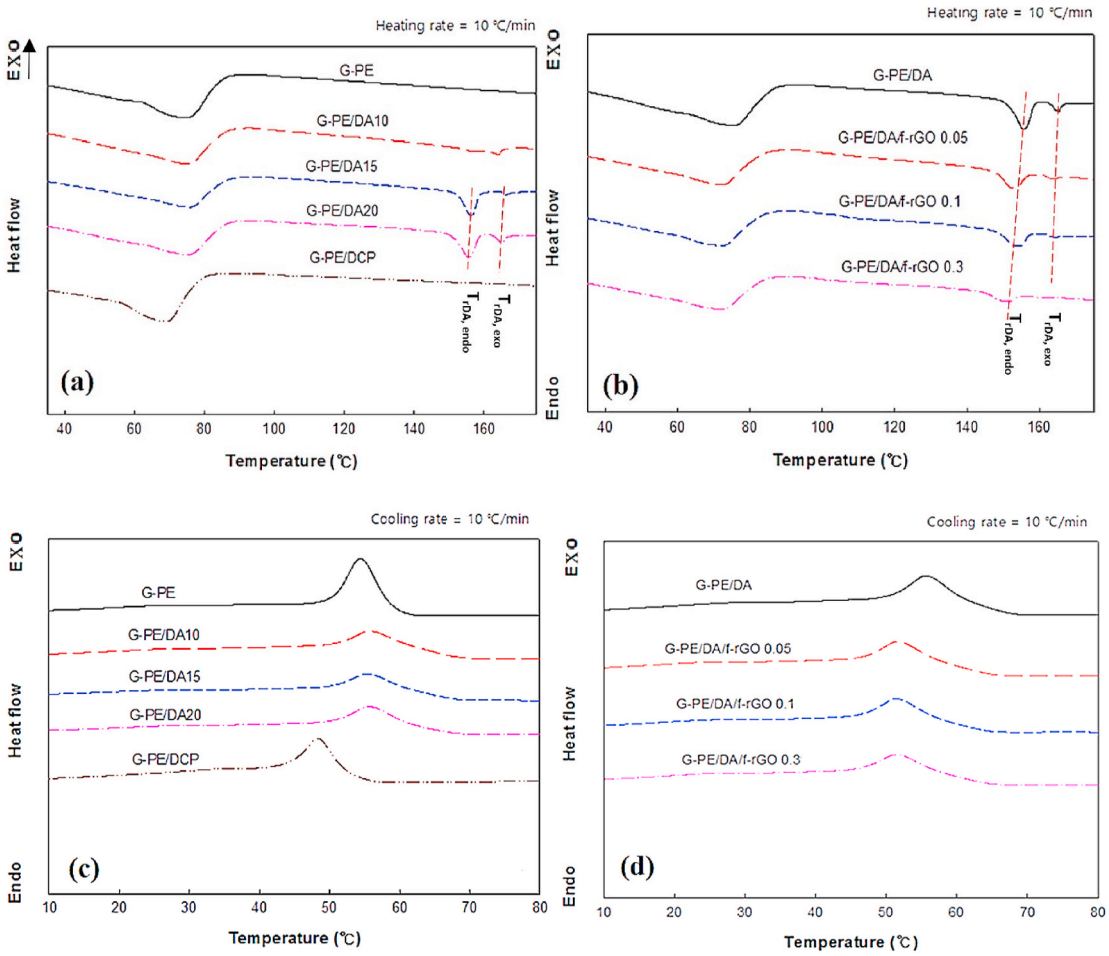

Fig. 9. (a) and (b) heating scans, (c) and (d) cooling scans of DSC thermograms of samples.

Table 1
Thermal properties of samples obtained from DSC thermograms.

Sample	Heating scan				Cooling scan	
	T_m (°C)	ΔH_m (J/g)	T_{rDA} (°C)	ΔH_{rDA} (J/g)	T_c (°C)	ΔH_c (J/g)
Neat G-PE	75.28	18.81	0	0	54.44	17.350
G-PE/DA10	75.35	17.85	157.26	0.138	56.11	9.014
G-PE/DA15	75.88	16.67	156.29 & 158.51	1.889 & 0.115	55.75	9.739
G-PE/DA20	75.42	15.49	155.57 & 158.12	2.581 & 0.254	55.87	9.738
G-PE/DCP	69.51	17.27	–	–	48.41	13.550
G-PE/DA/f-rGO 0.05	72.38	13.16	152.70 & 155.81	1.626 & 0.119	51.96	8.052
G-PE/DA/f-rGO 0.1	72.55	13.34	153.01 & 154.80	1.483 & 0.082	51.74	7.681
G-PE/DA/f-rGO 0.3	72.65	13.96	149.93	0.894	51.46	6.463

bended into a temporary U-like shape (θ_o), and then quenching to 0 °C for fixing the temporary shape for 10 min. After that, the external force was removed at room temperature and the fixed angle (θ_i) was measured. Finally, the shape recovery process was examined either by direct heating at 80 °C or by exposure of the samples to near infrared (NIR) light irradiation (an infrared lamp with an intensity of 65 mW/cm^2 containing a red filter that was placed at 30 cm away from the sample, Model Infraphil PAR 38E, Philips, Germany), and the final angle (θ_f) was recorded. The shape fixity (R_f) and recovery (R_r) ratios of samples were calculated using equations (2) and (3), respectively.

$$R_f = \frac{\theta_i}{\theta_0} \times 100\% \quad (2)$$

$$R_r = \frac{(\theta_i - \theta_f)}{\theta_0} \times 100\% \quad (3)$$

Thermally activated shape memory effect was also visually investigated in tensile mode using dog-bone-shaped specimens. First, the sample with an initial length of L_i was kept isothermally at 80 °C for 5 min, followed by stretching to 100% of its initial length (L_u) and then quenching to 0 °C for 10 min to fix the temporary shape. Afterward, the applied stress was removed and the length of sample was recorded (L_s). Upon heating the stretched samples either by direct heating at 80 °C or by NIR irradiation (same as above-mentioned set up), their original shape (L_r) recovered. The R_f and R_r values of samples were calculated using equations (4) and (5), respectively.

$$R_f = \frac{L_s - L_i}{L_u - L_i} \times 100\% \quad (4)$$

$$R_r = \frac{L_s - L_r}{L_s - L_i} \times 100\% \quad (5)$$

Shape memory properties of the samples were also quantitatively measured using DMA under a tensile mode using rectangular specimens ($30 \times 6 \times 0.8$ mm^3) as follows: (i) heating the sample with a rate of 3 °C/min and isothermal holding at 80 °C, (ii) applying a stress of 0.35 MPa, (iii) cooling to 0 °C with a rate of 3 °C/min, and equilibrating at this temperature while keeping the stress constant, (iv) fixing the temporary shape by removing the stress, and (v) recovering the original shape with

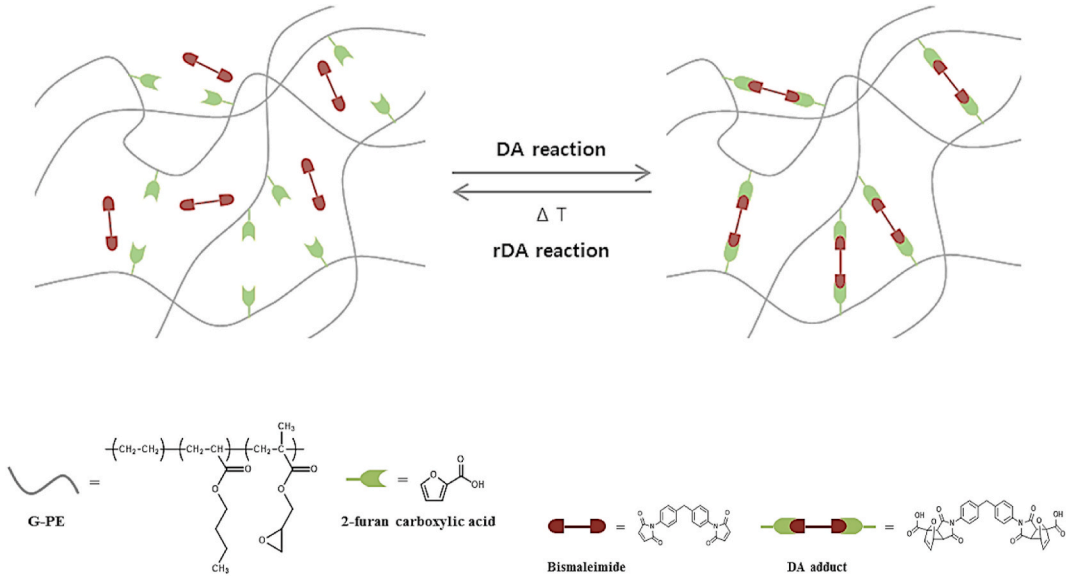

Fig. 10. Schematic illustration of the thermal reversibility feature of the crosslinked G-PE network through DA and rDA reactions.

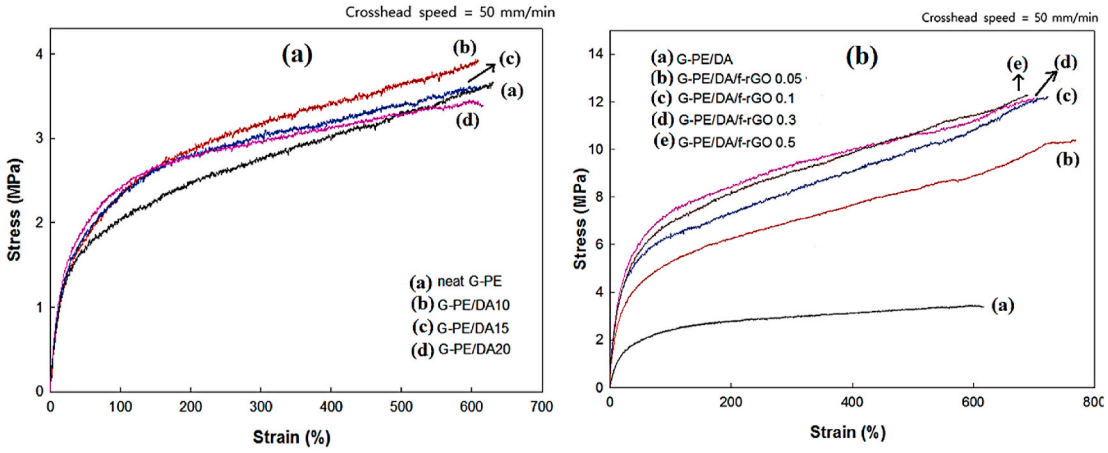

Fig. 11. Tensile stress-strain curves of (a) G-PE/DA networks and (b) G-PE/DA/f-rGO nanocomposites.

Table 2
Tensile properties of G-PE/DA networks and (b) G-PE/DA/f-rGO nanocomposites.

Sample	Modulus (MPa)	Tensile strength (MPa)	Elongation at break (%)
Neat G-PE	2.04	3.66	630.9
G-PE/DA10	2.32	3.93	609.6
G-PE/DA15	2.35	3.62	612.2
G-PE/DA20	2.41	3.38	616.8
G-PE/DA/f-rGO 0.05	5.28	10.40	769.2
G-PE/DA/f-rGO 0.1	6.41	12.02	723.3
G-PE/DA/f-rGO 0.3	7.37	12.15	700.5

a continuous heating to 80 °C at 3 °C/min. This cycle was repeated two times for each sample. The shape fixing ratio (R_f) and recovery ratio (R_r) of samples were determined using equations (6) and (7), respectively [13]:

$$R_f(N)\% = \frac{\varepsilon}{\varepsilon_{load}} \times 100 \quad (6)$$

$$R_r(N)\% = \frac{\varepsilon(N) - \varepsilon_{rec}(N)}{\varepsilon(N) - \varepsilon_{rec}(N-1)} \times 100 \quad (7)$$

where ε_{load}, ε, ε_{rec} and N indicate for the maximum strain before unloading, the strain upon unloading, the permanent strain after shape recovery, and the cycle number, respectively.

3. Results and discussion

3.1. Structural analyses

Fig. 3 shows FT-IR spectra of GO, f-GO, and f-rGO. The characteristic peaks of GO appeared at 1710 cm^{-1} (-C═O carboxyl stretching vibration), 1385 cm^{-1} (C–OH stretching), 1066 cm^{-1} (C–O–C of epoxide groups), and a wide peak from 3000 to 3500 cm^{-1} which was assigned to hydroxyl groups. All of these peaks originated from the oxygen-bearing functional groups were almost diminished in the f-rGO spectrum (Fig. 3 (c)), which reveals successful reduction of the GO [10]. The spectra of f-GO and f-rGO showed peaks at 2919, 2848, and 720 cm^{-1}, attributing to asymmetric and symmetric stretching, and rocking of $–CH_2$- chain of ODA on GO, respectively. In addition, new peaks located at 1564 cm^{-1} (N–H bending vibration) and 1465 cm^{-1} (C–N bending vibration) are

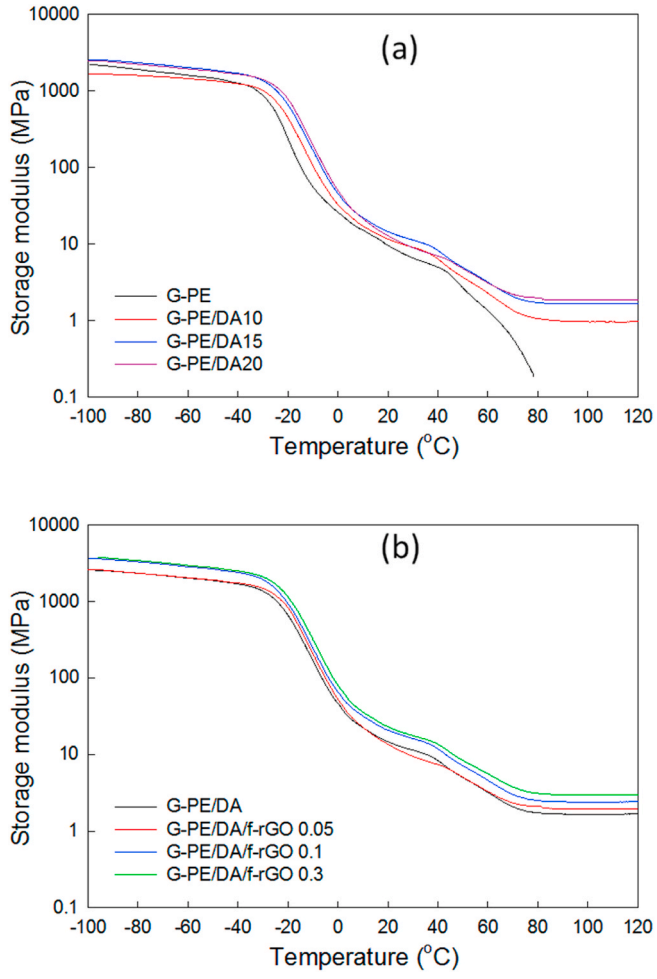

Fig. 12. Storage modulus of (a) G-PE/DA networks and (b) G-PE/DA/f-rGO nanocomposites as a function of temperature.

Table 3
Storage modulus at 100 °C and crosslink density (υ_d) of samples obtained from DMA.

Sample	E′ at 100 °C (MPa)	$\upsilon_d \times 10^4$ (mol/cm^3)
Neat G-PE	–	–
G-PE/DA10	0.96	1.1
G-PE/DA15	1.68	1.8
G-PE/DA20	1.81	1.9
G-PE/DA15/f-rGO 0.05	1.93	2.1
G-PE/DA15/f-rGO 0.1	2.38	2.6
G-PE/DA15/f-rGO 0.3	2.95	3.2

originated from the formed -C–NH–C- bonds as a result of the reaction between amine groups of ODA and epoxide groups of GO [36].

Fig. 4 shows FT-IR spectra of 2-furan carboxylic acid, bismaleimide, and DA adduct. The most important change after the DA reaction was the disappearance of out-of-plane hydrogen bending of furan ring at 753 cm^{-1}, which can be correlated to the fact that the furan ring was reacted with bismaleimide [37]. In addition, –C═O stretching vibration of the carboxylic acid groups at 1682 cm^{-1}, C═C stretching vibration of furan ring at 1516 cm^{-1}, C–O stretching vibration of carboxylic acid of DA adduct at 1299 cm^{-1}, and the peaks in the range of 3050–3450 cm^{-1} attributed to the hydroxyl group of carboxylic acid were observed [38,39]. The typical peaks of bismaleimide at 1702 and 1509 cm^{-1} were also appeared in the spectrum of DA adduct (Fig. 4 (c)).

The structure of DA adduct was also investigated by ^{1}H NMR, as shown in Fig. 5. The characteristic chemical shifts of DA adduct were appeared at 5.38 (H-1), 6.78 (H-2 and H-3), 3.57 and 3.62 (H-4 and H-5 of endo adduct, respectively), and 3.12 and 3.39 ppm (H-4 and H-5 of exo adduct, respectively) [40–43]. Meanwhile, the characteristic peaks of 2-furan carboxylic acid at 7.65 (H-A), 6.57 (H–B), and 7.34 ppm (H–C) [40] and the peak of bismaleimide located at 7.16 ppm (H-D) [41] were almost disappeared in the spectrum of DA adduct.

The structure of DA crosslinked G-PE was investigated by FT-IR. As shown in Fig. 6 (c), the intensity of epoxide group band at 910 cm^{-1} decreased [6,44] and the –OH stretching peak of furan carboxylic acid was almost disappeared after crosslinking. These results indicate that the reaction between epoxide and carboxylic acid groups happened, yielding a crosslinked ethylene copolymer network containing DA couplings.

3.2. Microstructure analyses

The cross-sectional FESEM micrographs of G-PE/DA/f-rGO nanocomposites containing various amounts of f-rGO were shown in Fig. 7. It can be seen that f-rGO nanoplatelets were tightly integrated within the G-PE/DA matrix. Samples showed a layered morphology with irregular fracture surfaces, especially at high graphene loading. Interfacial debonding at the filler–polymer interfaces during the fracture created numerous cracks throughout the samples. The multiple crack propagation and diversion led to rough fracture surfaces [45].

In addition, FE-TEM images of nanocomposites were shown in Fig. 8. It is evident that the f-rGO nanoplatelets were fairly dispersed in the nanocomposites due to good compatibility between the octadecylamine chains grafted on f-rGO and the G-PE matrix.

3.3. DSC analysis

DSC thermograms of samples were shown in Fig. 9, and their corresponding data were listed in Table 1. It can be seen from Fig. 9 that the melting and crystallization behaviors of samples were slightly changed with the addition of DA adduct. However, Fig. 9 (a) indicates that during the heating of DA adduct crosslinked G-PE samples, additional endothermic peak(s) appeared at high temperatures, while, neither the neat G-PE nor the DCP crosslinked sample (G-PE/DCP) exhibited any endothermic peaks in this temperature area. These endothermic peaks can be attributed to the de-crosslinking of G-PE molecular chains through retro Diels-Alder (rDA) reaction at T_{rDA} during the heating of samples [33], as illustrated in Fig. 10. Some samples exhibited two endothermic peaks in this area (indicated by dashed lines); one peak in a temperature range of 155.57–157.26 °C followed by a relatively smaller peak observed at a slightly higher temperature attributed to the rDA reaction of endo and exo isomers of DA adduct at $T_{rDA,\ endo}$ and $T_{rDA,\ exo}$, respectively [46,47]. The amount of endo moieties are often higher as compared to exo structures, especially when an electron withdrawing substituent presents on the furan and/or the maleimide ring [46].

Moreover, Table 1 indicates that the enthalpy of rDA reaction (ΔH_{rDA}) increased from 0 to 2.581 J/g as the content of endo DA adduct raised from 0 to 20 phr (Table 1), which can be correlated to the increase in the number of DA crosslinks with raising the DA adduct content in the samples [42].

Thermal characterization of G-PE/DA/f-rGO nanocomposites was also performed using DSC measurements. From Table 1 one can see that the melting temperature of G-PE/DA/f-rGO nanocomposites was slightly shifted to a lower temperature. During the heating of the nanocomposites loaded with 0.05 and 0.1 wt% f-rGO, two endothermic peaks in the ranges of 149.93–152.70 and 154.80–155.81 °C were observed, indicating that de-crosslinking of the G-PE network by rDA reaction of endo and exo moieties of DA adduct, respectively. Moreover, Fig. 9 (b) shows that with the increase in f-rGO content, the rDA peaks were shifted to a lower temperature, meanwhile, ΔH_{rDA} of nanocomposites was decreased with raising f-rGO loading. It seems that the amount of

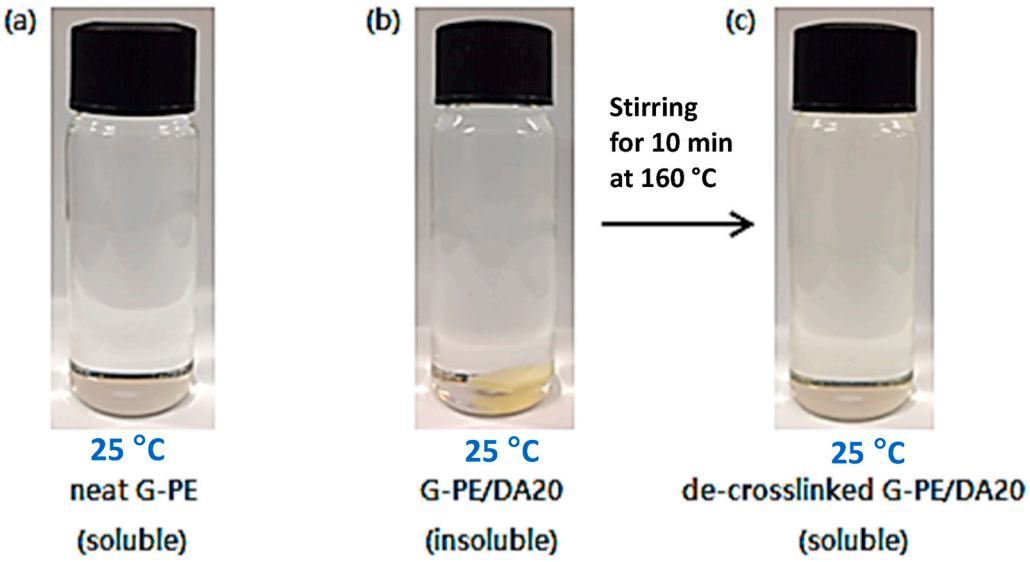

Fig. 13. Solubility test of (a) non-crosslinked, (b) DA crosslinked, and (c) de-crosslinked G-PE/DA20 in toluene.

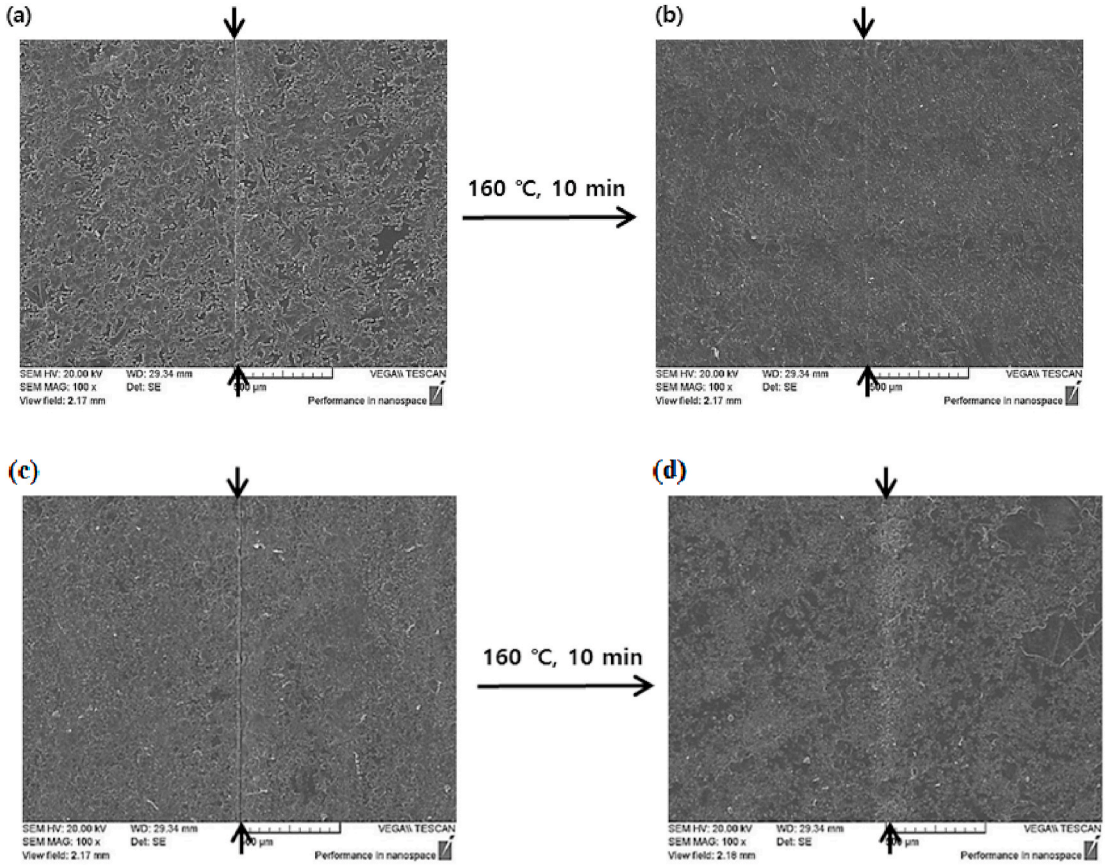

Fig. 14. SEM images of (a) scratched and (b) healed G-PE/DA20 network, (c) scratched and (d) healed G-PE/DA/f-rGO after healing at 160 °C for 10 min.

DA reaction between furan and bismaleimide was reduced with incorporation of f-rGO nanoplatelets.

3.4. Mechanical properties

The tensile stress-strain curves of samples were showed in Fig. 11, and the obtained data were listed in Table 2. Fig. 11 (a) indicates that the modulus of samples was slightly increased in the presence of DA adduct, while their elongation at break slightly reduced as compared to neat G-PE, which might be correlated to enhanced cross-link density. Besides, the tensile strength of G-PE/DA matrix did not change noticeably with incorporation of DA adduct.

The tensile stress-strain curves of G-PE/DA and its corresponding nanocomposites containing 0.05, 0.1, and 0.3 wt% of f-rGO were compared in Fig. 11 (b), and their corresponding mechanical properties were summarized in Table 2.

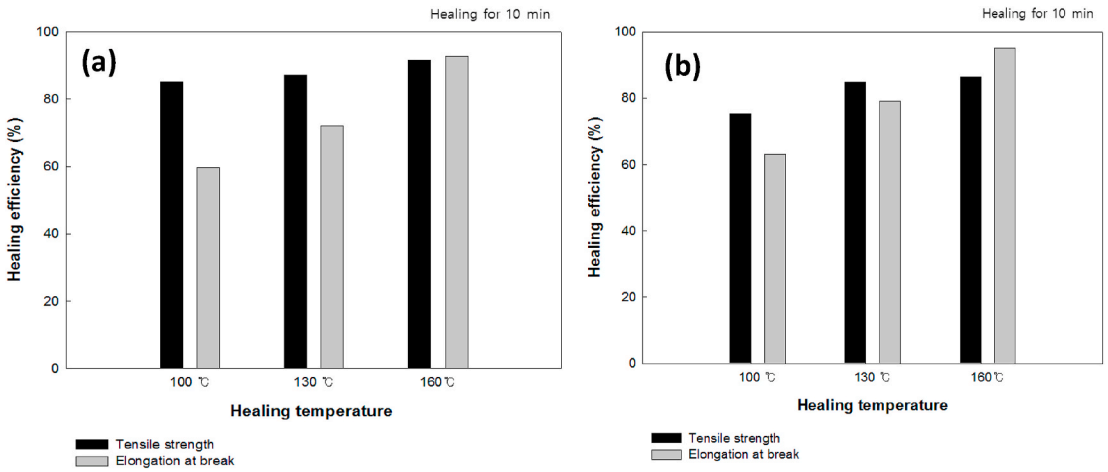

Fig. 15. The healing efficiency of (a) G-PE/DA20 network and (b) G-PE/DA/f-rGO 0.3 nanocomposite after healing at various temperatures for 10 min.

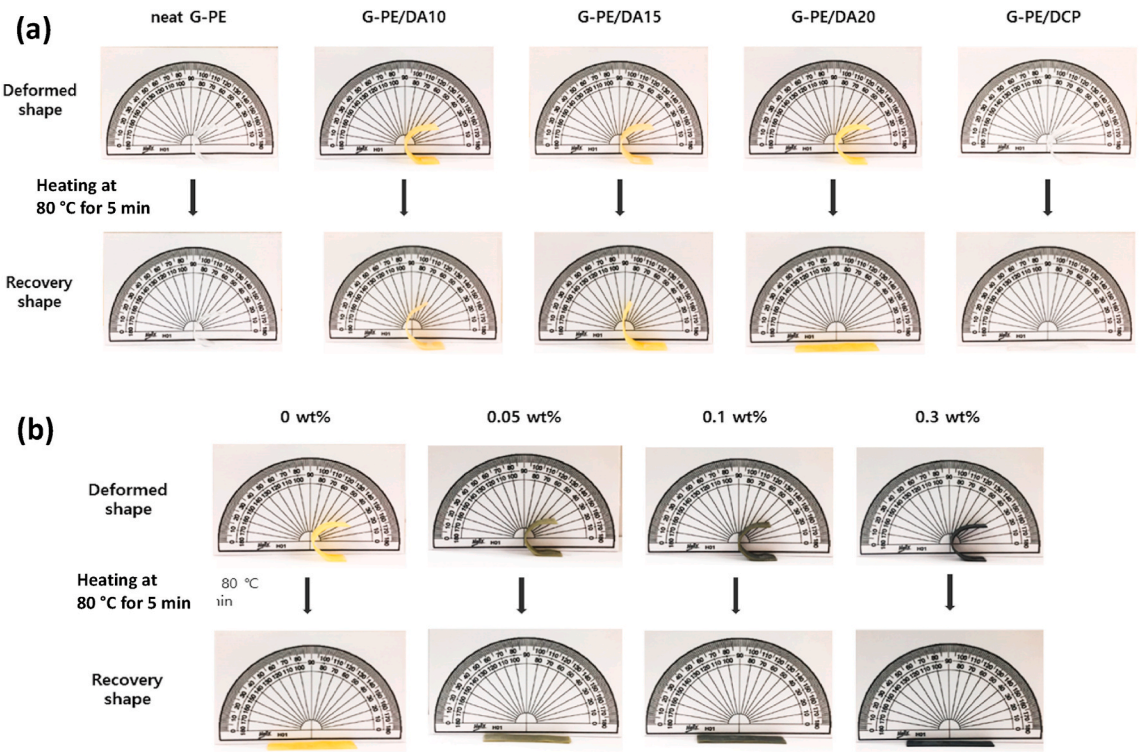

Fig. 16. Thermally triggered shape recovery behavior of U-like shape bended (a) neat G-PE, DA crosslinked samples and (b) G-PE/DA/f-rGO nanocomposites.

It is evident from Table 2 that with incorporation of small amount of f-rGO (as low as 0.05 wt%), the mechanical properties of the G-PE/DA matrix were noticeably and simultaneously improved (modulus from 2.41 to 5.28 MPa, tensile strength from 3.38 to 10.40 MPa, and elongation at break from 616.8 to 769.2%). This phenomena can be correlated to the well-dispersion of f-rGO and good compatibility and interface between the G-PE/DA matrix and the alkyl functionalized rGO (see Figs. 7 and 8), leading to large stress transfer from the polymer matrix to the nano fillers during the deformation process [45,48]. The modulus, tensile strength, and elongation at break of G-PE/DA/f-rGO 0.3 nanocomposite reached to ≈306, 359, and 114% of those of unfilled matrix, respectively. Nevertheless, the nanocomposite with 0.05 wt% of f-rGO exhibited maximum elongation at break and further increases in graphene content led to decrease of that which might be originated from the enhanced f-rGO agglomeration at high filler concentrations.

3.5. DMA results

Fig. 12 shows the variation of storage modulus with temperature. All of the samples except neat G-PE showed a rubbery plateau above T_m indicating that they are crosslinked. The storage modulus of rubbery plateau region (E′ at 100 °C) can be correlated with the crosslink density (υ_d) of samples. The crosslink density of the samples calculated using equation (1) and E′ at 100 °C values were shown in Table 3. It can be seen that crosslink density was increased with increasing DA content and reached saturated when DA content is 15 phr, implying DA adduct can act as a crosslinking agent for the G-PE.

3.6. Reprocessing ability of samples

The reversibility of the G-PE network crosslinked by DA adduct was

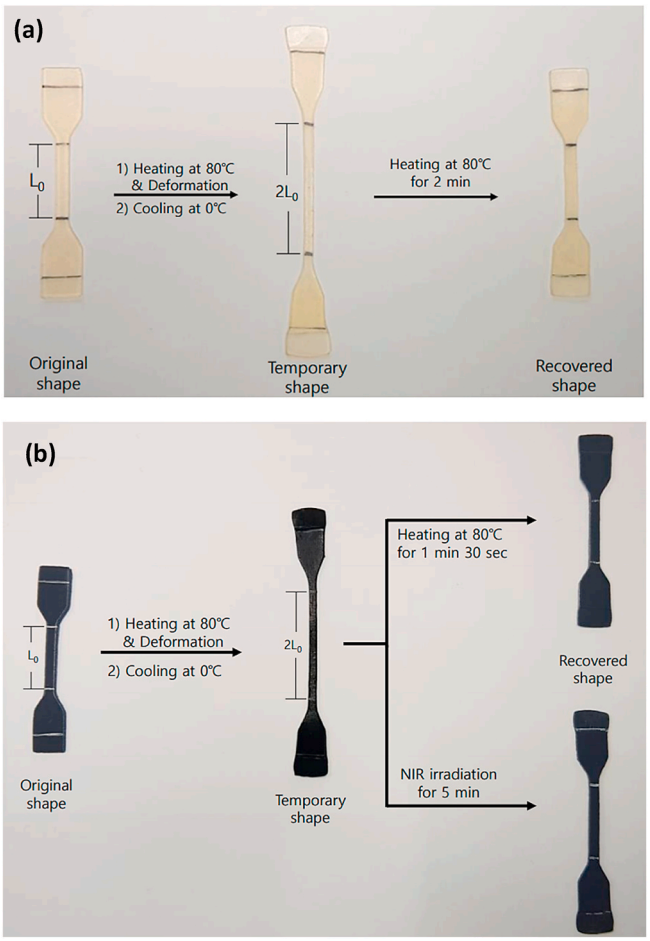

Fig. 17. (a) Thermally triggered shape recovery of stretched G-PE/DA20, (b) thermally and NIR triggered shape memory effects of stretched G-PE/DA/f-rGO 0.3 nanocomposite.

Table 4
Thermally triggered shape memory properties of G-PE, G-PE/DA networks, and G-PE/DA/f-rGO nanocomposites.

Sample	Bending		Tensile	
	R_f (%)	R_r (%)	R_f (%)	R_r (%)
Neat G-PE	100.0	0.7	100.0	0.7
G-PE/DA10	98.7	20.0	98.7	92.0
G-PE/DA15	100.0	34.0	99.2	94.0
G-PE/DA20	100.0	100.0	96.5	99.5
G-PE/DCP	99.3	99.3	99.3	99.5
G-PE/DA/f-rGO 0.05	99.3	99.3	99.3	99.7
G-PE/DA/f-rGO 0.1	98.7	98.7	98.7	98.8
G-PE/DA/f-rGO 0.3	100.0	100.0	99.0	100.0

visually investigated by the solubility test. The non-crosslinked G-PE was soluble in toluene at room temperature (Fig. 13 (a)). However, the crosslinked G-PE/DA network did not dissolve in toluene but swelled at room temperature (Fig. 13 (b)). Upon heating to 160 °C, the swollen crosslinked polymer was completely dissolved and a pale yellow solution was obtained (Fig. 13 (c)), indicating that high temperature causes in de-crosslinking of sample by rDA reaction (Fig. 10).

It was also indicated that a crosslinked sheet of G-PE/DA20 and G-PE/DA/f-rGO 0.3 samples can be recycled to produce a new sheet through compression molding at a temperature above T_{rDA}. The cut specimen pieces were reprocessed at 160 °C for 10 min and annealed at 50 °C for 3 days, which lead to dissociation and reformation of DA bonds, respectively. Interestingly, Fig. S1 and Table S2 show that both remolded G-PE/DA20 and G-PE/DA/f-rGO 0.3 samples have almost the same mechanical properties as their corresponding original samples even after second processing cycle, which can be attributed to the reformation of broken DA bonds during the annealing process at 50 °C.

3.7. Scratch-healing property of samples

A scratch with ≈60% of the thickness of specimen was created in the middle of samples using a razor blade (Fig. 14 (a) and (c)). The scratch healing property of the G-PE/DA20 and G-PE/DA/f-rGO 0.3 samples was then investigated by SEM observations. The sheet with surface scratch was heated at 160 °C for 10 min. As shown in Fig. 14 (b) and (d), the scratch of both samples almost disappeared after heating, indicating that the samples can be healed at high temperature.

The healing efficiency of the G-PE/DA20 and G-PE/DA/f-rGO 0.3 samples at various temperatures was quantitatively investigated by comparing the mechanical properties of original sample with its corresponding healed sample (after annealing at 50 °C for 3 days), and the results were shown in Fig. 15 and Table S3. It can be seen that the healing efficiency of both samples in terms of the tensile strength and elongation at break recoveries was increased with raising the healing temperature. For instance, the tensile strength recovery of G-PE/DA20 and G-PE/DA/f-rGO 0.3 samples increased from 85.21 to 91.57% and from 63.09 to 95.22% when the healing temperature was raised from 100 to 160 °C, respectively. This indicates that both samples have an excellent healing behavior above their T_{rDA}, as the tensile strength of the healed G-PE/DA20 and G-PE/DA/f-rGO 0.3 was already up to 91.57 and 95.22% of the strength of their corresponding original samples after 10 min healing at 160 °C, respectively.

The scratch/crack healing mechanism comprises simultaneous shape memory and self-healing functionalities of SMPs [49], which called Diels–Alder shape-memory assisted self-healing (DASMASH) in SMPs linked by DA reaction [27]; closure of scratch with the assistance of their shape memory effect above their thermal transition temperature (T_m in our case), and then diffusion of the polymer chains across the area of damage and re-association of broken DA bonds and physical links [31, 50]. The DA bonds are immobilized through crystallite phase below T_m, and are activated to a highly dynamic state above T_m causing in the re-association of broken bonds with T_m triggered shape memory effect that facilitates the closure of scratch and accordingly reformation of the broken DA bonds during the scratching process [26].

When the temperature was increased to 100 and then to 130 °C, which are well above the T_m of samples, the polymer chain mobility was progressively increased leading to a faster diffusion of the polymer molecular chains across the scratch and, as a result, a higher mechanical properties recovery through the reformation of DA bonds. However, with further raising the healing temperature above the $T_{rDA,}$ of samples, i.e., 160 °C, a large number of free furan and bismaleimide moieties will be available on the scratch surface to heal the scratch of samples during the cooling process. In addition, G-PE/DA/f-rGO 0.3 nanocomposite displayed higher healing efficiency as compared to G-PE/DA20 at 160 °C. The migration of polymer chains across damaged interface and re-adsorption onto the surface of neighboring graphene can be assumed as an additional healing mechanism of nanocomposites [51,52]. In addition, the heat transfer rate is relatively high in the nanocomposites containing the thermal conductive graphene, which can accelerate the heat induced healing process.

3.8. Thermal and NIR triggered shape memory effects of samples

Thermally activated shape memory behavior of U-like shape bended as well as stretched specimen of samples was represented in Figs. 16 and 17. The shape fixing ratio (R_f) and shape recovery ratio (R_r) of neat G-PE, G-PE/DA samples and their corresponding G-PE/DA/f-rGO nanocomposites samples were listed in Table 4. It can be seen that all of the samples displayed excellent fixing ratios. The neat G-PE could not

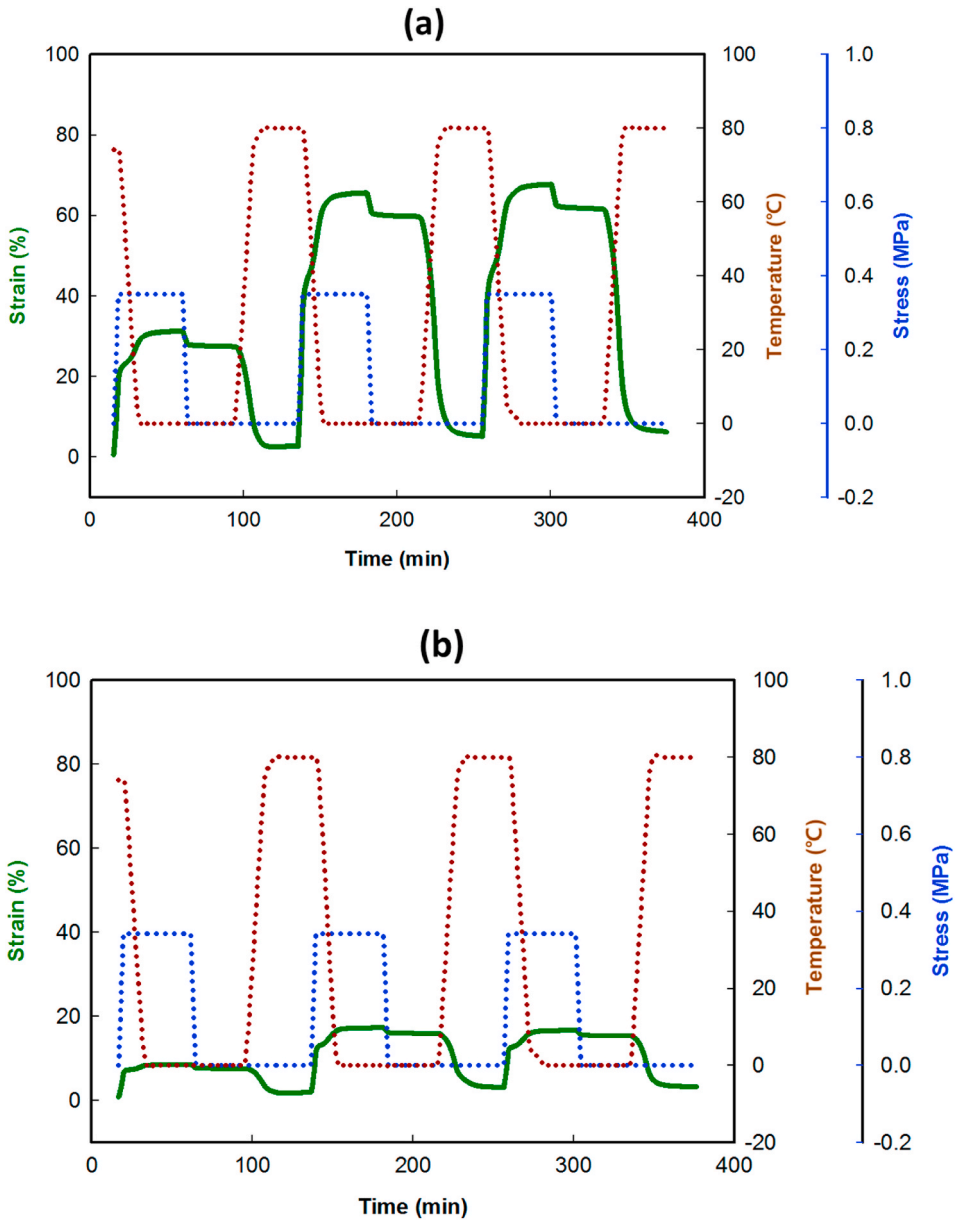

Fig. 18. Shape memory cycles of (a) G-PE/DA20 (b) G-PE/DA20/f-rGO samples obtained by DMA.

Table 5
Shape fixing ratio and shape recovery ratio of G-PE/DA20 and G-PE/DA20/f-rGO 0.3 determined by DMA.

Sample	R_f (2)%	R_f (3)%	R_r (2)%	R_r (3)%
G-PE/DA20	92.4	92.6	96.2	96.6
G-PE/DA20/f-rGO 0.3	97.3	97.4	98.2	98.1

display shape recovery as shown in Fig. 16. This is most likely due low Young's modulus and low storable strain in the neat G-PE sample [53,54]. While, it is evident from Table 4 that R_r of G-PE was remarkably improved with incorporation DA adduct. As, the bended as well as the stretched G-PE/DA20 and its G-PE/DA/f-rGO nanocomposites could almost fully recover to their original shape. For comparison, shape recovery behavior of DCP linked G-PE was also examined under the same condition and it exhibited an R_r value of 99.3%.

Fig. S2 compares thermally triggered shape memory behaviors of the original and reprocessed G-PE/DA20 samples. Table S4 shows that this sample could preserve its shape memory properties even after second reprocessing cycle. Moreover, Fig. S3 and Table S5 show thermally triggered shape memory properties of the original and reprocessed G-PE/DA/f-rGO 0.3 nanocomposite. This sample also could almost retain it shape fixing and recovery properties after two cycle processing.

Heat induced shape memory properties of G-PE/DA20 and G-PE/DA/f-rGO 0.3 were also determined during three consecutive cycles using DMA, as shown in Fig. 18 (a) and (b), respectively. To avoid residual stresses from the processing history of the samples, R_f and R_r values were calculated based on second and third cycles, and the results are summarized in Table 5. It can be seen that R_f and R_r values of G-PE/DA20 were improved in the presence of f-rGO nanofillers.

In semicrystalline G-PE with covalently crosslinked structure, the crystalline region of G-PE acts as a reversible (switch) phase providing shape fixity capacity, while the covalently crosslinked network of G-PE serves as fixing phase, which "memorizes" the original shape after deformation during heating process [24,55]. Besides, f-rGO nanoplatelets can be considered as an additional fixing phase in the nanocomposites [31].

It should be noted that the shape recovery was happened well below

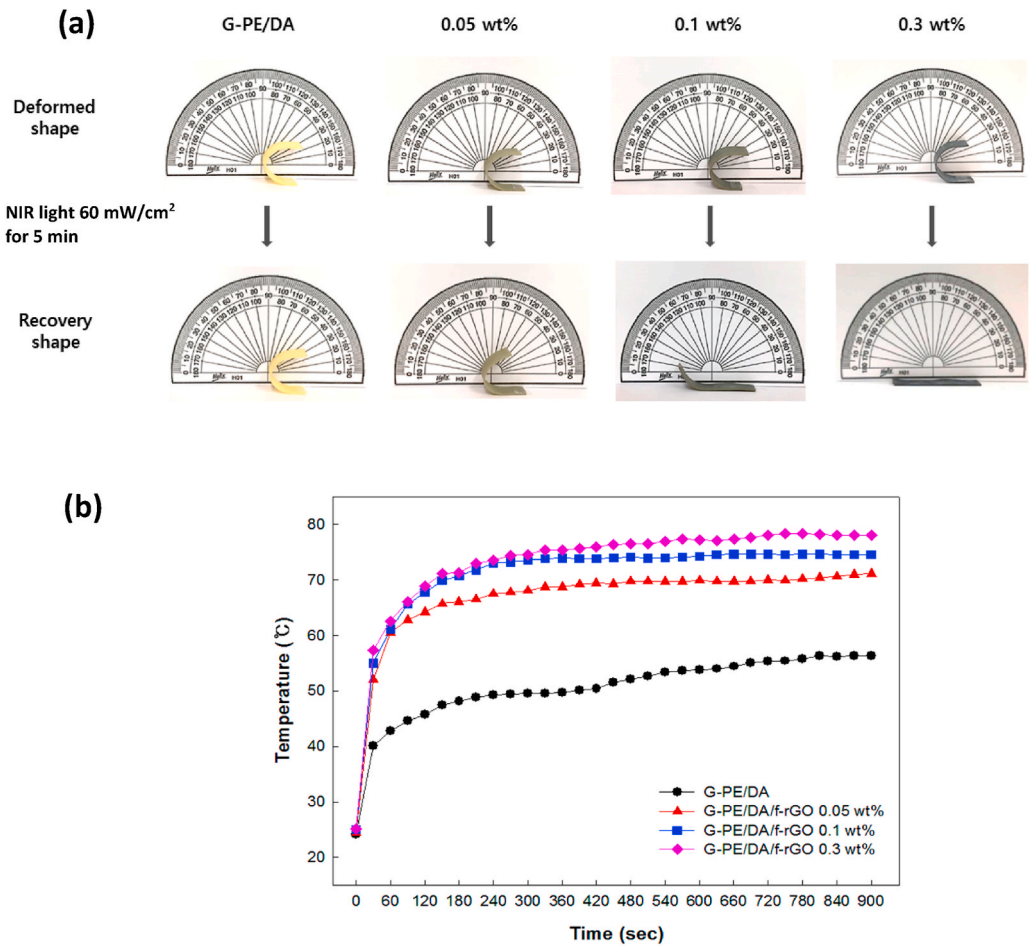

Fig. 19. (a) Thermally and (b) NIR triggered shape memory effects of G-PE/DA20 and G-PE/DA/f-rGO nanocomposites, and (c) variation in the surface temperature of G-PE/DA and G-PE/DA/f-rGO nanocomposites during time upon exposure to NIR light.

Table 6
NIR triggered shape memory properties of G-PE/DA20 and its G-PE/DA/f-rGO nanocomposites.

Sample	Bending		Tensile	
	R_f (%)	R_r (%)	R_f (%)	R_r (%)
G-PE/DA20	100.0	0.0	100.0	0.0
G-PE/DA/f-rGO 0.05	99.3	19.7	99.3	79.7
G-PE/DA/f-rGO 0.1	98.7	89.3	98.7	94.3
G-PE/DA/f-rGO 0.3	100.0	100.0	99.0	100.0

the rDA of samples, where the DA bonds were preserved [26]. Therefore, all of the DA covalent netpoints acted as "permanent crosslinks" fixing the original shape, whereas the crystallites of G-PE played as a reversible phase that freeze the polymer network within the temporary shape [56]. Upon heating to above T_m, the crystallites of G-PE are melted and accordingly the recovery of permanent shape happens due to the release of stored entropy and rearrangement of the polymer molecular chains to a higher entropy state [53,54].

The improvement in R_f and R_r values with the increase in DA adduct content as well as f-rGO loading might stem from greater increment in entropy during the shape recovery process of the DA crosslinked nanocomposites, inducing a large recovery force upon the temperature of sample exceeds the T_m of G-PE crystallites.

Although there are many known stimuli to activate SMPs, NIR light has the unique advantages of localized, non-contact, remote actuation, and also easy switching on-off for triggering [2]. Due to high photothermal conversion efficiency of f-rGO, it can provide NIR light-triggered shape memory capability to the matrix [10]. Upon exposure of the sample to NIR light, the embedded f-rGO nanoplatelets convert NIR light into thermal-energy throughout the polymer matrix and raise its temperature up to melting of the crystallites, and accordingly lead to release of the trapped entropy and recovery of permanent shape [11].

NIR triggered shape memory effect of U-like shape samples were shown Fig. 19 (a). In addition, NIR triggered shape recovery of the stretched G-PE/DA/f-rGO 0.3 nanocomposite was typically shown in 17 (b). Fig. 19 (a) exhibits that the G-PE/DA network did not show any NIR induced shape recovery effect. While, the nanocomposites displayed shape recovery effect with radiation of NIR on the sample as a result of the photothermal effect of graphene [10]. As, the bended and stretched G-PE/DA/f-rGO 0.3 nanocomposite samples demonstrated excellent NIR induced shape recovery values of 99.0 and 100%, respectively (Table 6).

Fig. 19 (b) shows the variation of the surface temperature of G-PE/DA and G-PE/DA/f-rGO nanocomposites versus irradiation time of NIR light. It is evident that the surface temperature of nanocomposites (especially those containing 0.1 and 0.3 wt% f-rGO) abruptly increased when they were exposed to NIR irradiation. However, the surface temperature of the unfilled G-PE/DA could not raise over its T_m within the investigated period of time due to lack of graphene in this sample.

4. Conclusion

In this work, chemically crosslinked polyethylene copolymer containing thermo-reversible DA bonds was successfully prepared by a melt blending and a subsequent thermal molding. It was observed that with

loading of f-rGO as low as 0.05 wt%, the mechanical properties of the G-PE/DA matrix are noticeably improved (modulus from 2.41 to 5.28 MPa, tensile strength from 3.38 to 10.40 MPa, and elongation at break from 616.8 to 769.2%), which was attributed to well-dispersion of f-rGO and good compatibility between the matrix and f-rGO. Besides, G-PE/DA20 and its corresponding nanocomposites showed excellent shape fixity and recovery ratios in response to direct heating above their T_m. The reprocessing experiments revealed that the mechanical properties and shape memory effects of the remolded samples were approximately same as original samples, which was attributed to the reformation of DA bonds during the annealing process. Besides that, it was shown that the shape memory behavior of the developed nanocomposites could also be activated upon exposure to NIR radiation due to excellent photothermal effect of f-rGO.

In addition, the crosslinked PE samples indicated an excellent heat activated scratch-healing behavior (healing efficiency up to 91.57%) owing to their SM effect and reversibility of crosslink points, which was further improved with loading of f-rGO nanoplatelets (healing efficiency up to 95.22%). The combination of strong mechanical properties, recyclability, and thermo-healing capability of the developed SM nanocomposites, along with their facile preparation from a commercially available polymer, can make them as a promising SM material for diverse applications, such as fast deployable and actuating devices.

Author statement

Kyung Hee Kang: Validation, Investigation, Resources, Writing - Original Draft. Young-Wook Chang: Conceptualization, Development or design of methodology, Validation, Writing - Review & Editing, Supervision, Project administration, Funding acquisition. Mohammad Sabzi: Data Curation, Investigation, Writing - Original Draft, Writing - Review & Editing, Visualization.

Declaration of competing interest

The authors have no conflicts of interest to declare.

Acknowledgement

This work was supported by Korea Institute for Advancement of Technology (KIAT) (Project No: P0008458, The Competency Development Program for Industry Specialist).

Appendix A. Supplementary data

Supplementary data to this article can be found online at https://doi.org/10.1016/j.polymertesting.2021.107383.

References

[1] J.-C. Kim, Y.-W. Chang, M. Sabzi, Designing self-crosslinkable ternary blends using epoxidized natural rubber (ENR)/poly (ethylene-co-acrylic acid)(EAA)/poly (ε-caprolactone)(PCL) demonstrating triple-shape memory behavior, Eur. Polym. J. 152 (2021) 110488.
[2] M. Sabzi, N. Shafagh, M. Mohammadi, Assembly of gelatin biopolymer to fibrous sepiolite clay for efficient dye removal from wastewater, J. Appl. Polym. Sci. 136 (2019) 48266.
[3] M. Keramati, I. Ghasemi, M. Karrabi, H. Azizi, M. Sabzi, Dispersion of graphene nano platelets in poly lactic acid with the aid of a zwitterionic surfactant: evaluation of the shape memory behavior, Polym. Plast. Technol. Eng. 55 (2016) 1039–1047.
[4] M. Keramati, I. Ghasemi, M. Karrabi, H. Azizi, M. Sabzi, Incorporation of surface modified graphene nanoplatelets for development of shape memory PLA nanocomposite, Fibers Polym. 17 (2016) 1062–1068.
[5] M. Babaahmadi, M. Sabzi, G.R. Mahdavinia, M. Keramati, Preparation of amorphous nanocomposites with quick heat triggered shape memory behavior, Polymer 112 (2017) 26–34.
[6] M. Kashif, Y.-W. Chang, Triple-shape memory effects of modified semicrystalline ethylene–propylene–diene rubber/poly (ε-caprolactone) blends, Eur. Polym. J. 70 (2015) 306–316.
[7] Y. Wang, J. Liu, L. Xia, M. Shen, Z. Xin, Super-tough poly (lactic acid) thermoplastic vulcanizates with heat triggered shape memory behaviors based on modified natural Eucommia ulmoides gum, Polym. Test. 80 (2019) 106077.
[8] L. Wang, J. Hua, Z. Wang, Facile design of heat-triggered shape memory ethylene-vinyl acetate copolymer/nitrile-butadiene thermoplastic vulcanizates via zinc dimethacrylate induced interfacial compatibilization, Polym. Test. 76 (2019) 481–489.
[9] O. León, A. Muñoz-Bonilla, D. Soto, D. Pérez, M. Rangel, M. Colina, M. Fernández-García, Removal of anionic and cationic dyes with bioadsorbent oxidized chitosans, Carbohydr. Polym. 194 (2018) 375–383.
[10] M. Kashif, Y.-W. Chang, Supramolecular hydrogen-bonded polyolefin elastomer/modified graphene nanocomposites with near infrared responsive shape memory and healing properties, Eur. Polym. J. 66 (2015) 273–281.
[11] W. Du, Y. Jin, L. Shi, Y. Shen, S. Lai, Y. Zhou, NIR-light-induced thermoset shape memory polyurethane composites with self-healing and recyclable functionalities, Compos. B Eng. (2020) 108092.
[12] M. Sabzi, M. Babaahmadi, N. Samadi, G.R. Mahdavinia, M. Keramati, N. Nikfarjam, Graphene network enabled high speed electrical actuation of shape memory nanocomposite based on poly (vinyl acetate), Polym. Int. 66 (2017) 665–671.
[13] M. Sabzi, M. Babaahmadi, M. Rahnama, Thermally and electrically triggered triple-shape memory behavior of poly (vinyl acetate)/poly (lactic acid) due to graphene-induced phase separation, ACS Appl. Mater. Interfaces 9 (2017) 24061–24070.
[14] H. Yan, L. Li, X. Shi, J.-M. Yeh, Y. Wei, P. Zhang, Conductive stretchable shape memory elastomers combining with electrical stimulation for synergistic osteogenic differentiation, Polym. Test. (2020) 106672.
[15] N. Rogers, F. Khan, Characterization of deformation induced changes to conductivity in an electrically triggered shape memory polymer, Polym. Test. 32 (2013) 71–77.
[16] U.N. Kumar, K. Kratz, W. Wagermaier, M. Behl, A. Lendlein, Non-contact actuation of triple-shape effect in multiphase polymer network nanocomposites in alternating magnetic field, J. Mater. Chem. 20 (2010) 3404–3415.
[17] Z. He, N. Satarkar, T. Xie, Y.T. Cheng, J.Z. Hilt, Remote controlled multishape polymer nanocomposites with selective radiofrequency actuations, Adv. Mater. 23 (2011) 3192–3196.
[18] L. Xia, F. Yang, H. Wu, M. Zhang, Z. Huang, G. Qiu, Z. Xin, W. Fu, Novel series of thermal-and water-induced shape memory Eucommia ulmoides rubber composites, Polym. Test. 81 (2020) 106212.
[19] L. Xia, M. Zhang, H. Gao, G. Qiu, Z. Xin, W. Fu, Thermal-and water-induced shape memory Eucommia ulmoides rubber and microcrystalline cellulose composites, Polym. Test. 77 (2019) 105910.
[20] F. Katzenberg, J.C. Tiller, Shape memory natural rubber, J. Polym. Sci. B Polym. Phys. 54 (2016) 1381–1388.
[21] T. Raidt, R. Hoeher, F. Katzenberg, J.C. Tiller, Chemical cross-linking of polypropylenes towards new shape memory polymers, Macromol. Rapid Commun. 36 (2015) 744–749.
[22] R. Hoeher, T. Raidt, F. Katzenberg, J.C. Tiller, Heating rate sensitive multi-shape memory polypropylene: a predictive material, ACS Appl. Mater. Interfaces 8 (2016) 13684–13687.
[23] C.L. Lewis, E.M. Dell, A review of shape memory polymers bearing reversible binding groups, J. Polym. Sci. B Polym. Phys. 54 (2016) 1340–1364.
[24] F. El Feninat, G. Laroche, M. Fiset, D. Mantovani, Shape memory materials for biomedical applications, Adv. Eng. Mater. 4 (2002) 91–104.
[25] K. Inoue, M. Yamashiro, M. Iji, Recyclable shape-memory polymer: poly (lactic acid) crosslinked by a thermoreversible Diels–Alder reaction, J. Appl. Polym. Sci. 112 (2009) 876–885.
[26] L.T. Nguyen, H.Q. Pham, D.T.T. Phung, T.T. Truong, H.T. Nguyen, T.C.D. Doan, C. M. Dang, H. Le Tran, P.T. Mai, D.T. Tran, Macromolecular design of a reversibly crosslinked shape-memory material with thermo-healability, Polymer 188 (2020) 122144.
[27] G. Rivero, L.-T.T. Nguyen, X.K. Hillewaere, F.E. Du Prez, One-pot thermo-remendable shape memory polyurethanes, Macromolecules 47 (2014) 2010–2018.
[28] S. Thomas, A. Surendran, Self-Healing Polymer-Based Systems, Elsevier, 2020.
[29] M. Bednarek, P. Kubisa, Reversible networks of degradable polyesters containing weak covalent bonds, Polym. Chem. 10 (2019) 1848–1872.
[30] T. Raidt, R. Hoeher, M. Meuris, F. Katzenberg, J.C. Tiller, Ionically cross-linked shape memory polypropylene, Macromolecules 49 (2016) 6918–6927.
[31] M. Sabzi, M. Babaahmadi, N. Samadi, G.R. Mahdavinia, M. Keramati, N. Nikfarjam, Graphene network enabled high speed electrical actuation of shape memory nanocomposite based on poly (vinyl acetate), Polym. Int. 66 (2017) 665–671.
[32] Z. Lin, Y. Liu, C.-p. Wong, Facile fabrication of superhydrophobic octadecylamine-functionalized graphite oxide film, Langmuir 26 (2010) 16110–16114.
[33] N. Bai, K. Saito, G.P. Simon, Synthesis of a diamine cross-linker containing Diels–Alder adducts to produce self-healing thermosetting epoxy polymer from a widely used epoxy monomer, Polym. Chem. 4 (2013) 724–730.
[34] C. Cai, Y. Zhang, X. Zou, R. Zhang, X. Wang, Q. Wu, P. Sun, Rapid self-healing and recycling of multiple-responsive mechanically enhanced epoxy resin/graphene nanocomposites, RSC Adv. 7 (2017) 46336–46343.
[35] P. Raffa, A. Kassi, J. Gosschalk, N. Migliore, L.M. Polgar, F. Picchioni, A structure-properties relationship study of self-healing materials based on styrene and furfuryl methacrylate cross-linked via diels–alder chemistry, Macromol. Mater. Eng. 306 (2021) 2000755.
[36] W. Li, X.-Z. Tang, H.-B. Zhang, Z.-G. Jiang, Z.-Z. Yu, X.-S. Du, Y.-W. Mai, Simultaneous surface functionalization and reduction of graphene oxide with octadecylamine for electrically conductive polystyrene composites, Carbon 49 (2011) 4724–4730.

[37] L.M. Polgar, G. Fortunato, R. Araya-Hermosilla, M. van Duin, A. Pucci, F. Picchioni, Cross-linking of rubber in the presence of multi-functional cross-linking aids via thermoreversible Diels-Alder chemistry, Eur. Polym. J. 82 (2016) 208–219.
[38] C.-H. Huang, Y.-L. Liu, Self-healing polymeric materials for membrane separation: an example of a polybenzimidazole-based membrane for pervaporation dehydration on isopropanol aqueous solution, RSC Adv. 7 (2017) 38360–38366.
[39] P. Tanasi, M.H. Santana, J. Carretero-González, R. Verdejo, M.A. López-Manchado, Thermo-reversible crosslinked natural rubber: a Diels-Alder route for reuse and self-healing properties in elastomers, Polymer 175 (2019) 15–24.
[40] K.-S. Byun, W.J. Choi, H.-Y. Lee, M.-J. Sim, S.-H. Cha, J.-C. Lee, The effect of electron density in furan pendant group on thermal-reversible Diels–Alder reaction based self-healing properties of polymethacrylate derivatives, RSC Adv. 8 (2018) 39432–39443.
[41] X. Liu, P. Du, L. Liu, Z. Zheng, X. Wang, T. Joncheray, Y. Zhang, Kinetic study of Diels–Alder reaction involving in maleimide–furan compounds and linear polyurethane, Polym. Bull. 70 (2013) 2319–2335.
[42] T. Ikeda, D. Oikawa, T. Shimasaki, N. Teramoto, M. Shibata, Organogelation behavior, thermal and mechanical properties of polymer network formed by the Diels–Alder reaction of furan-and maleimide-terminated four-arm star-shaped ε-caprolactone oligomers, Polymer 54 (2013) 3206–3216.
[43] P. Du, M. Wu, X. Liu, Z. Zheng, X. Wang, P. Sun, T. Joncheray, Y. Zhang, Synthesis of linear polyurethane bearing pendant furan and cross-linked healable polyurethane containing Diels–Alder bonds, New J. Chem. 38 (2014) 770–776.
[44] S. Wu, J. Li, G. Zhang, Y. Yao, G. Li, R. Sun, C. Wong, Ultrafast self-healing nanocomposites via infrared laser and their application in flexible electronics, ACS Appl. Mater. Interfaces 9 (2017) 3040–3049.
[45] M. Sabzi, L. Jiang, M. Atai, I. Ghasemi, PLA/sepiolite and PLA/calcium carbonate nanocomposites: a comparison study, J. Appl. Polym. Sci. 129 (2013) 1734–1744.
[46] V. Froidevaux, M. Borne, E. Laborbe, R. Auvergne, A. Gandini, B. Boutevin, Study of the Diels–Alder and retro-Diels–Alder reaction between furan derivatives and maleimide for the creation of new materials, RSC Adv. 5 (2015) 37742–37754.
[47] K. Ishida, Y. Furuhashi, N. Yoshie, Synthesis of Diels–Alder network polymers from bisfuranic terminated poly (l-lactide) and tris-maleimide, Polym. Degrad. Stabil. 110 (2014) 149–155.
[48] M. Keramati, I. Ghasemi, M. Karrabi, H. Azizi, M. Sabzi, Dispersion of graphene nanoplatelets in polylactic acid with the aid of a zwitterionic surfactant: evaluation of the shape memory behavior, Polym. Plast. Technol. Eng. 55 (2016) 1039–1047.
[49] H. Wei, Y. Yao, Y. Liu, J. Leng, A dual-functional polymeric system combining shape memory with self-healing properties, Compos. B Eng. 83 (2015) 7–13.
[50] H.B. Nejad, J.M. Robertson, P.T. Mather, Interwoven polymer composites via dual-electrospinning with shape memory and self-healing properties, MRS Communications 5 (2015) 211.
[51] N. Samadi, M. Sabzi, M. Babaahmadi, Self-healing and tough hydrogels with physically cross-linked triple networks based on Agar/PVA/Graphene, Int. J. Biol. Macromol. 107 (2018) 2291–2297.
[52] G. Gao, G. Du, Y. Sun, J. Fu, Self-healable, tough, and ultrastretchable nanocomposite hydrogels based on reversible polyacrylamide/montmorillonite adsorption, ACS Appl. Mater. Interfaces 7 (2015) 5029–5037.
[53] G. Fei, G. Li, L. Wu, H. Xia, A spatially and temporally controlled shape memory process for electrically conductive polymer–carbon nanotube composites, Soft Matter 8 (2012) 5123–5126.
[54] M. Anthamatten, S. Roddecha, J. Li, Energy storage capacity of shape-memory polymers, Macromolecules 46 (2013) 4230–4234.
[55] Q. Zhao, H.J. Qi, T. Xie, Recent progress in shape memory polymer: new behavior, enabling materials, and mechanistic understanding, Prog. Polym. Sci. 49 (2015) 79–120.
[56] M. Kashif, Y.W. Chang, Supramolecular semicrystalline polyolefin elastomer blends with triple-shape memory effects, Polym. Int. 65 (2016) 577–583.